Strong spin–phonon coupling between a single-molecule magnet and a carbon nanotube nanoelectromechanical system

Marc Ganzhorn[1], Svetlana Klyatskaya[2], Mario Ruben[2,3] and Wolfgang Wernsdorfer[1]★

Magnetic relaxation processes were first discussed for a crystal of paramagnetic transition ions[1]. It was suggested that mechanical vibrations of the crystal lattice (phonons) modulate the crystal electric field of the magnetic ion, thus inducing a 'direct' relaxation between two different spin states[1–3]. Direct relaxation has also been predicted for single-molecule magnets with a large spin and a high magnetic anisotropy[1,4–7] and was first demonstrated in a Mn_{12} acetate crystal[8]. The spin-lattice relaxation time for such a direct transition is limited by the phonon density of states at the spin resonance[1]. In a three-dimensional system, such as a single-molecule magnet crystal, the phonon energy spectrum is continuous, but in a one-dimensional system, like a suspended carbon nanotube, the spectrum is discrete and can be engineered to an extremely low density of states[9]. An individual single-molecule magnet, coupled to a suspended carbon nanotube, should therefore exhibit extremely long relaxation times[9] and the system's reduced size should result in a strong spin–phonon coupling[10,11]. Here, we provide the first experimental evidence for a strong spin–phonon coupling between a single molecule spin and a carbon nanotube resonator, ultimately enabling coherent spin manipulation and quantum entanglement[10,11].

Carbon nanotubes (CNT) have become an essential building block for nanoelectromechanical systems (NEMS). Their low mass and high Young's modulus give rise to high oscillation frequencies for transverse[12,13] and longitudinal modes[14–16], therefore enabling ground-state cooling with state-of-the-art cryogenics and a large zero point motion in the quantum regime[17]. Moreover, the strong coupling between nanomechanical motion and single-electron tunnelling in high-Q CNT NEMS allows electronic actuation and detection of the nanomechanical motion[18–21]. As such, CNT NEMS can be used for ultrasensitive mass sensing[22–24] or as magnetic torque detectors for single spin systems[25].

A single spin, strongly coupled with a CNT NEMS in the quantum regime, could serve as an elementary qubit in quantum information processing. It has been suggested recently that a strong coupling between a quantum CNT NEMS and a single electron spin would enable basic qubit control and the implementation of entangled states[9]. In this framework, coupling a single-molecule magnet (SMM) to the quantized nanomechanical motion of a CNT NEMS is a very attractive option[26]. Chemical engineering allows the synthesis of perfectly identical SMMs, as well as their integration into nanoscale devices such as electromigrated junctions[27–29] or CNT transistors[30]. A large magnetic moment and a strong, uniaxial magnetic anisotropy enable, for instance, quantum tunnelling of magnetization[31,32] or quantum phase

interference[33], yielding coherence times on the order of microseconds in crystalline form[34]. Moreover, it was recently predicted that the spin–phonon coupling between an SMM and a quantum CNT NEMS is strong enough to allow coherent spin manipulation and quantum entanglement of a spin and a resonator[10,11]. In this Letter, we first present the SMM and CNT NEMS. We then establish a strong spin–phonon coupling between the two systems, that is, between an individual $TbPc_2$-SMM and the quantized high-Q longitudinal stretching mode (LSM) of the CNT resonator. The strong spin–phonon coupling presented here would enable the quantum control of magnetization at a single-phonon level[9,10] and the entanglement of a single spin with quantized mechanical motion[9,11].

We study the magnetization reversal of a pyrene-substituted bis(phthalocyaninato)terbium(III) SMM (hereafter $TbPc_2$, Fig. 1a) grafted to a CNT resonator[36]. The $TbPc_2$ is a rare earth SMM in which the magnetic moment is carried by a single Tb^{3+} ion sandwiched between two organic phthalocyanine (Pc) ligand planes[35]. The $TbPc_2$ has a $S = 1/2$ radical delocalized over the Pc ligand planes. As a result of π–π interaction, this radical can easily hybridize with the π electrons of any form of sp^2 carbon without affecting the magnetic properties of the Tb^{3+} ion[30,36,37]. The highly anisotropic $4f$ shell of the Tb^{3+} ion and its intrinsically strong spin–orbit coupling result in a magnetic ground state of $J = 6$ and a pronounced uniaxial magnetic anisotropy (Fig. 1a). The ground-state doublet $J_z = \pm 6$ is separated from the excited states by several hundreds of kelvin, which makes the $TbPc_2$ an Ising-like spin system at low temperatures ($T < 5$ K) and small magnetic fields ($B < 10$ T)[35]. A strong hyperfine interaction with the nuclear spin $I = 3/2$ of the Tb^{3+} ion splits the ground-state doublet $J_z = \pm 6$ into four states each (Fig. 1b). Finally, the ligand field generates a small transverse magnetic anisotropy resulting in avoided level crossings (black circles in Fig. 1b)[35].

At cryogenic temperatures, magnetization reversal can occur through two different processes. Around zero magnetic field, the avoided level crossings allow for quantum tunnelling of magnetization $|J_z,I_z\rangle \rightarrow |-J_z,I_z\rangle$ (refs 30,35). At high magnetic fields the magnetization reverses through a direct relaxation process involving non-coherent tunnelling events combined with the emission of a phonon[30] (Fig. 1b). Previous experiments on $TbPc_2$ single crystals[35] and on $TbPc_2$ coupled to a non-suspended CNT[30] have shown that the spin relaxation was mainly enabled by bulk phonons in the environment of an individual SMM (crystal or substrate). However, an individual $TbPc_2$-SMM grafted onto a suspended CNT is physically decoupled from the bulk phonons in the substrate or the transistor leads. As a consequence, the $TbPc_2$-SMM can only couple to one-dimensional phonons, associated with the

---

[1]Institut Néel, CNRS et Université Joseph Fourier, BP 166, F-38042 Grenoble Cedex 9, France, [2]Institute of Nanotechnology (INT), Karlsruhe Institute of Technology (KIT), 76344 Eggenstein-Leopoldshafen, Germany, [3]Institut de Physique et Chimie des Matériaux de Strasbourg (IPCMS), CNRS-Université de Strasbourg, 67034 Strasbourg, France. *e-mail: wolfgang.wernsdorfer@grenoble.cnrs.fr
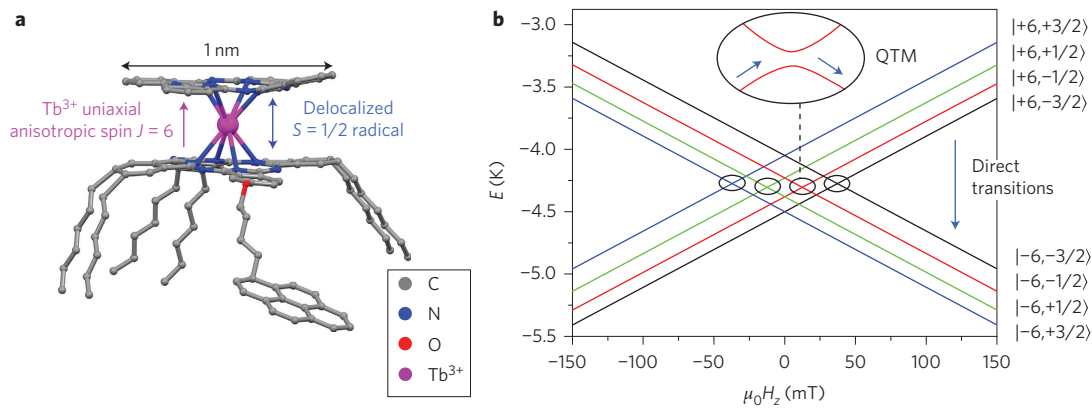
Figure 1 | Rare-earth SMM. a, Schematic representation of a pyren-substituted TbPc$_2$-SMM. A Tb^{3+} ion (pink) is sandwiched between two organic phthalocyanine (Pc) ligand planes. Owing to the highly anisotropic 4f shell of the Tb^{3+} ion and strong spin–orbit coupling, the TbPc$_2$ can be considered as an Ising-like spin system, with high magnetic anisotropy and a ground-state doublet $J_z = \pm 6$. The oxidation state of the Tb^{3+} ion generates a spin $S = 1/2$ radical delocalized over the phthalocyanine planes. **b**, Zeeman diagram presenting the energy E of the two ground states $J_z = \pm 6$ as a function of the magnetic field $\mu_0 H_z$. The strong hyperfine coupling with the nuclear spin $I = 3/2$ in the Tb^{3+} ion splits the ground-state doublet $J_z = \pm 6$ into four states. The corresponding Zeeman diagram reveals four avoided level crossings (black circles) around zero field, allowing for QTM $|J_z, I_z\rangle \rightarrow |-J_z, I_z\rangle$. Alternatively, magnetization reversal can occur through a direct relaxation process, involving the excitation of a phonon.

nanomechanical motion of the CNT. It was recently demonstrated that high-frequency and high-Q transverse[12] and longitudinal phonon[14–16] modes in a CNT at cryogenic temperatures should be quantized, thus yielding a discrete phonon energy spectrum.

Single-electron tunnelling (SET) onto the CNT quantum dot shifts the equilibrium position of the CNT along the axis of the CNT by an amount proportional to the electron–phonon coupling g (ref. 14). For an intermediate electron–phonon coupling $g \approx 1$, the electron therefore effectively tunnels into an excited vibrational state (Fig. 2b). If the tunnel rate Γ_{out} is larger than the relaxation rate γ into the vibrational ground state, the electron tunnels out of the dot, resulting in equidistant excited states in the region of SET, running parallel to the edge of the Coulomb diamond (black arrows, Fig. 2c)[14,15]. For large electron–phonon coupling $g \gg 1$, one also observes a current suppression at low bias, a phenomenon known as Franck–Condon blockade[16]. It was also demonstrated that one can pump excited vibrational states in a Coulomb-blockade regime by means of higher-order co-tunnelling processes[15].

For the device studied in this Letter, we observe a spectrum of equidistant excited states in the region of SET (black arrows, Fig. 2c), with an average energy separation of $\hbar\omega = 140\ \mu\text{eV} = 1.5\ \text{K}$ (Fig. 2d). According to $\hbar\omega = 110\ \mu\text{eV}/L\ [\mu\text{m}]$ (ref. 14) this corresponds to an oscillator length of $L = 800\ \text{nm}$, which is consistent with the length of the CNT quantum dot, $L_D = 850\ \text{nm}$ (Fig. 2a). From the current intensity of these excited states we can estimate the electron–phonon coupling g (Fig. 2d) using the following equation[16]:

$$\Delta I \propto \frac{e^{-g} g^n}{n!} \qquad (1)$$

where n is the phonon quantum number. We obtain $g = 0.6 \pm 0.3$, which is comparable to the results of previous experiments[14]. Finally, we can estimate a lower boundary for the quality factor of this longitudinal phonon[15]. The quality factor is given by $Q = \omega/(2\pi\gamma)$, where γ is the relaxation rate into the ground state. For the vibrational states to be visible in a SET, we should have $\Gamma_{\text{out}} > \gamma$. The tunnel current at the edge of the Coulomb diamond $I \approx 50\ \text{pA}$ gives an approximation of the tunnelling rate $\Gamma_{\text{out}} \approx 310\ \text{MHz}$. Hence, the quality factor yields $Q > \omega/(2\pi\Gamma_{\text{out}}) \approx 110$, corresponding to a phonon linewidth of the order of 15 mK. We now demonstrate that this high-Q longitudinal phonon mode can be activated by
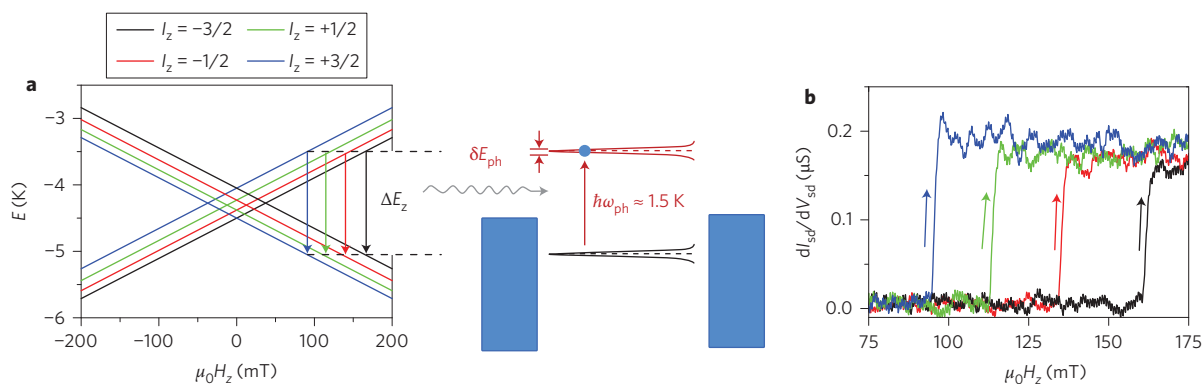
the magnetization reversal of a single TbPc$_2$, thus revealing strong spin–phonon coupling.

First, we tune our CNT quantum dot to a regime of Coulomb blockade ($V_{\text{sd}} = 0$, $V_{\text{lg}} = 16.5\ \text{mV}$). In a regime of strong spin–phonon coupling, the magnetization reversal of an individual TbPc$_2$-SMM via direct transition can induce the excitation of this longitudinal stretching mode phonon on the CNT quantum dot (Fig. 3a). The linewidth of the high-Q phonon was estimated to be on the order of 15 mK and is therefore smaller than the energy level spacing $\delta E_z = 120$, 150 and 180 mK between the nuclear spin states of the Tb^{3+} ion[29,35]. Consequently, we should observe four different direct transitions matching the phonon energy $\hbar\omega = 1.5\ \text{K}$, that is, four switching fields at 89, 113, 137 and 161 mT, corresponding to the different nuclear spin states of the Tb^{3+} ion (Fig. 3a). By sweeping the magnetic field component parallel to the TbPc$_2$ easy axis, we can induce magnetization reversal of the Tb^{3+} ion. As described by Urdampilleta *et al.*[30], reversal of the SMM causes an abrupt increase in the differential conductance through the CNT quantum dot, thus enabling an electronic readout and revealing the four switching fields of the Tb^{3+} ion (Fig. 3b). Note that the field sweep direction was previously aligned with the TbPc$_2$ easy axis (see Supplementary Information).

We performed magnetic field sweeps along the TbPc$_2$ easy axis at a rate of 50 mT s^{-1}, from negative to positive field values at different transverse magnetic fields $\mu_0 H_{\text{trans}}$, while monitoring the differential conductance in the CNT ($V_{\text{sd}} = 0$ and $V_{\text{lg}} = 16.5\ \text{mV}$). The magnetization reversal of the Tb^{3+} ion in a sweep translates as a jump in the differential conductance of the CNT, as described above (see also Fig. 3b). The corresponding magnetic field, the switching field $\mu_0 H_{\text{sw}}$, is extracted and plotted as a function of the transverse magnetic field $\mu_0 H_{\text{trans}}$ (Fig. 4a). The measurement reveals four switching fields between 80 and 160 mT, which are independent of the transverse magnetic field component $\mu_0 H_{\text{trans}}$. By reversing the field sweep direction, the TbPc$_2$ magnetization is reversed symmetrically between $-80\ \text{mT}$ and $-160\ \text{mT}$. To obtain a magnetization reversal statistic, we performed 200 sweeps back and forth at zero transverse magnetic field. The histogram of the extracted switching fields shows four dominant switching events at 88, 112, 137 and 160 mT with an average full-width at half-maximum (FWHM) of 2 mT (Fig. 4b). The model described in Fig. 3 predicts that in the case of a strong coupling between the TbPc$_2$ spin and the observed quantized longitudinal phonon mode in the CNT (energy $\hbar\omega = 1.5\ \text{K}$ and linewidth $\delta E_{\text{ph}} = 15\ \text{mK}$),
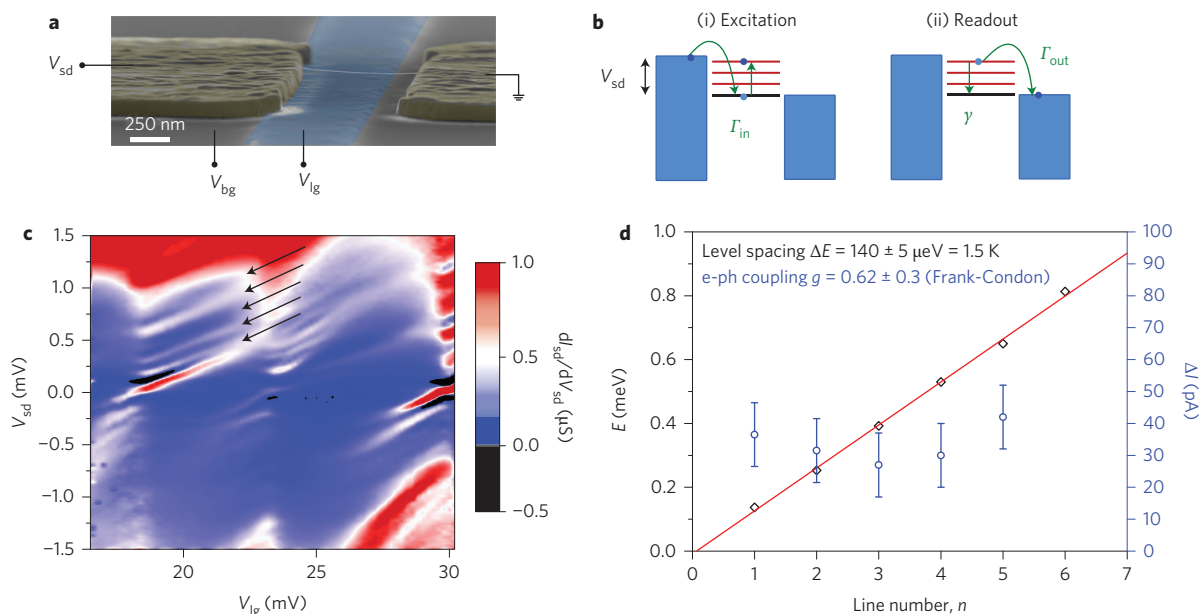
Figure 2 | Longitudinal stretching modes in CNT NEMS. a, False-colour SEM image of a CNT NEMS with local metallic (V_{lg}, blue) and Si++ (V_{bg}, grey) backgate. **b**, Actuation and detection of longitudinal stretching modes (LSM) of a CNT NEMS. (i) SET onto the suspended CNT shifts the equilibrium position of the CNT along its axis and proportional to the electron–phonon (e-ph) coupling g, leaving the electron in an excited vibrational state (red). (ii) If $\Gamma_{out} > \gamma$, the electron tunnels out of the dot, resulting in equidistant excited states running parallel to the edge of the Coulomb diamond (indicated by the black arrows in **c. c**, Stability diagram of the CNT showing the differential conductance as a function of gate and bias voltages at 20 mK and 1.4 T. The black arrows indicate the excited vibrational states attributed to an LSM, as described above. **d**, Energy of excited vibrational states (black diamonds) versus excitation line number n at $V_g = 18$ mV. A linear fit suggests an LSM frequency of $\hbar\omega = 140$ µeV, which is consistent with the CNT length of 850 nm (see text). From the maximum current intensity ΔI (blue circles) of the excited vibrational states we can estimate the LSM e-ph coupling factor as $g \approx 0.6 \pm 0.3$. Owing to measurement uncertainties in **c**, the relative error for ΔI is estimated to be 10%.


Figure 3 | Strong spin–phonon coupling of a TbPc₂-SMM and a CNT NEMS. a, The CNT quantum dot is tuned to a regime of Coulomb blockade ($V_{sd} = 0$, $V_{lg} = 16.5$ mV in Fig. 2c). The magnetization reversal of the TbPc₂ via direct transition results in excitation of the electron into a vibrational (LSM) state in the CNT resonator. In contrast to bulk phonons, the energy spectrum of an LSM phonon in one-dimensional CNTs is discretized and yields high quality factors around $Q \approx 1 \times 10^2$. The corresponding phonon linewidth $\delta E_{ph} \approx 15$ mK is smaller than the energy separation between the Tb^{3+} nuclear spin states $\Delta E_I > 120$ mK. Hence, we observe four different transitions, corresponding to the four nuclear spin states as depicted by the coloured arrows and a transition energy $\Delta E_z = \hbar\omega_{ph} = 1.5$ K. **b**, By sweeping the magnetic field component $\mu_0 H_z$ (parallel to the easy axis of the SMM), we induce magnetization reversal of the Tb^{3+} ion, resulting in an abrupt increase in the differential conductance through the dot. The switching field depends on the nuclear spin state occupied before magnetization reversal. The arrows depict the scan direction.

the magnetization reversal of the TbPc₂ will indeed occur from each of the four nuclear spin states of the Tb^{3+} ion at magnetic fields of 89, 113, 137 and 161 mT (Fig. 3). Also, the Zeeman energy corresponding to the FWHM of each switching event in Fig. 4b is ~30 mK, which is in close agreement with the phonon linewidth of $\delta E_{ph} = 15$ mK determined in the previous section. Moreover, all four switching events in the TbPc₂ have a transition energy of $\Delta E_z = 1.5$ K, which is in perfect agreement with the LSM phonon energy of $\hbar\omega = 1.5$ K. The experimental findings are thus in

excellent agreement with the provided model. The strong interaction between the molecular TbPc₂ spin and the quantized LSM phonon is further supported by the magnitude of the spin–phonon coupling, which we will evaluate in the following.

Finally, we can estimate the spin–phonon coupling between the magnetization of the TbPc₂-SMM and the quantized longitudinal phonon. For this purpose, we consider a TbPc₂-SMM rigidly grafted to the suspended CNT. Owing to the conservation of total angular momentum, the magnetization reversal of the Tb^{3+} ion

167
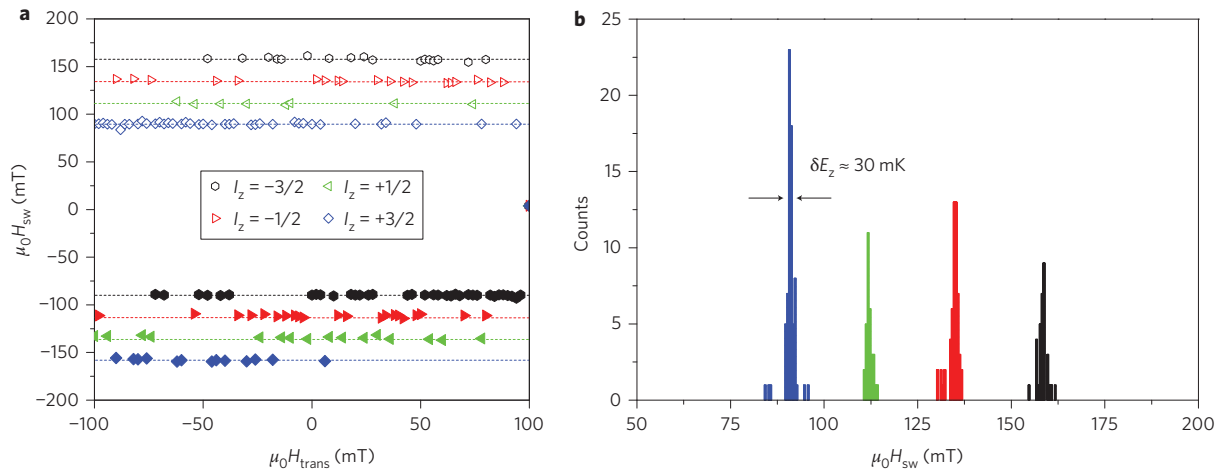
Figure 4 | Nuclear spin-dependent magnetization reversal of a single TbPc$_2$ coupled to a CNT NEMS. a, Switching field $\mu_0 H_{sw}$ versus transverse magnetic field component $\mu_0 H_{trans}$ for a sweep rate of 50 mT s^{-1}. We observe four distinct switching fields at positive values when sweeping the field from negative to positive values (open symbols) and at negative values when reversing the sweep direction (filled symbols). The switching does not depend on the transverse magnetic field component. We therefore attribute these events to the magnetization reversal of the Tb^{3+} ion via a nuclear spin-dependent direct transition enabled by strong spin–phonon coupling. No quantum tunnelling of magnetization was observed in our measurement. The dotted lines are to guide the eye. **b**, Histogram of the switching fields obtained for 200 field sweeps with a zero transverse magnetic field component for one sweep direction and a sweep rate of 50 mT s^{-1}. We observe four dominant switching events at 88, 112, 137 and 160 mT corresponding to the switching fields for the +3/2, +1/2, −1/2 and −3/2 nuclear spin states, respectively. The FWHM of the switching field yields $\delta B = 2$ mT and the corresponding Zeeman energy of $\delta E_z \approx 30$ mK is consistent with the phonon linewidth $\delta E_{ph} \approx 15$ mK.

causes a rotation of the molecule by an angle φ, in a plane perpendicular to its easy axis[10,11,38] (Supplementary Fig. S5). Because of the rigid grafting to the CNT, the lattice rotation of the SMM translates to a longitudinal stretching mode in the suspended CNT resonator beam[10,38]. The Hamiltonian of the hybrid SMM–resonator can be written as

$$H = H_{ph} + H_B + e^{-iJ_z\hat{\varphi}} H_{cf} e^{iJ_z\hat{\varphi}} \qquad (2)$$

where $H_{ph} = \hbar\omega_l(a^\dagger a + 1/2)$ corresponds to the energy of the quantized phonon mode and $H_B = g\mu_B B_z J_z$ is the Zeeman energy of the TbPc$_2$ (Supplementary Section S3). The last term describes the modification of crystal electric field (cf) by the rotation of the TbPc$_2$, where H_{cf} is the unperturbed crystal field and φ is the angle of rotation of the crystal lattice. Equation (2) can be reduced to an effective Jaynes–Cummings Hamiltonian (Supplementary Section S3):

$$H = H_{ph} + H_{cf} + H_B + \hbar g_{s-ph}(a + a^\dagger)O_4^{-4} \qquad (3)$$

where H_{ph} describes the free quantized longitudinal phonon mode, $H_{TbPc_2} = H_{cf} + H_B$ the TbPc$_2$-SMM in the absence of the phonon, a and $a^\dagger$ the creation and annihilation operators of the phonon mode and O_4^{4-} the Stevens spin operator of the TbPc$_2$-SMM. The spin–phonon coupling then yields (Supplementary Section S3)

$$g_{s-ph} = \frac{\beta A_4^4}{2}\sqrt{\frac{2\hbar}{I_z\omega}} \qquad (4)$$

with the moment of inertia of the TbPc$_2$-SMM is $I_z = 10^{-42}$ kg m^2, the phonon frequency is $\omega_l = 34$ GHz and the crystal field parameter is $\beta A_4^4 = 1.8$ mK. We therefore estimate the spin–phonon coupling to be $g_{s-ph} = 1.5$ MHz. A spin–resonator coupling of this magnitude could result in a suppression of quantum tunnelling of magnetization (QTM) on the SMM by nanomechanical quantum interference effects[10], the creation of coherent magneto-mechanical oscillations[10] or the entanglement of a single spin with quantum

mechanical oscillator[9,11]. We would like to point out that we did not observe QTM in our spin–resonator system. Although the absence of QTM could be related to nanomechanical quantum interference effects, as stated above, we do not have sufficient evidence to support such a claim. This would require further study, which is beyond the scope of this work.

In conclusion, we have demonstrated a strong spin–phonon coupling between a single molecular spin and the quantized, high-Q mechanical motion of a CNT resonator. It has been predicted that a coupling of this magnitude would induce strong non-linearities in the mechanical motion of a carbon nanotube, which can for instance be used to enhance the sensitivity of CNT-based magnetometers[9,25]. A sensitivity of a few μ_B is to be expected[25]. Moreover, the strong spin–phonon coupling would enable the electric manipulation of a single molecular spin by microwave irradiation[9]. Reciprocally, a strong spin–phonon interaction would allow the spin-based detection of the mechanical motion of the nanotube[39] or the ground-state cooling of the resonator by manipulating the molecular spin via electron spin resonance[9]. Ultimately, our results open the path to the quantum entanglement of a single spin and a quantized mechanical motion.

Methods

Sample preparation. A 1-μm-wide metallic local gate was patterned by optical deep-ultraviolet (DUV) lithography and subsequent electron-beam evaporation of molybdenum (20 nm) on a degenerately p-doped silicon wafer with a 300-nm-thick layer of thermal SiO$_2$. A layer of 100 nm of Al$_2$O$_3$ was then deposited by atomic layer deposition. Using optical DUV lithography and electron-beam evaporation of molybdenum (20 nm) and platinum (160 nm), source–drain electrodes were aligned above the local gate. Suspended CNTs were finally grown by chemical vapour deposition (CVD) at 800 °C from a CH$_4$ feedstock and iron/molybdenum catalyst spots patterned on the source–drain electrodes next to the junction. The CNT device length ranged from 800 nm to 1 μm. The pyrene-substituted TbPc$_2$ was synthesized as reported in ref. 36. TbPc$_2$ powder was dissolved in a solution of dichloromethane and dropcast onto the sample. The droplet was subsequently dried in a critical point dryer to avoid destruction of the suspended CNTs through capillary effects.

Low-temperature measurements. Conductance measurements were carried out in a He$_3$/He$_4$ dilution refrigerator with a base temperature of 20 mK. The refrigerator was equipped with two orthogonal magnetic fields coils, generating up

to 1.4 T and 0.5 T respectively for both coils, in the plane of the sample, with a maximum sweep rate of 250 mT s^{-1}. We could orient the field direction with respect to the easy axis of the TbPc$_2$-SMM by probing the magnetization reversal at different magnetic field angles (Supplementary Section S1). The field sweep rate and temperature dependences of the switching fields are presented in Supplementary Section S2. The transport measurements were made with an ADWIN real-time data acquisition system.

References

1. Abragam, A. & Bleaney, B. *Electron Paramagnetic Resonance of Transition Ions* (Oxford Univ. Press, 1970).
2. Heitler, W. & Teller, E. Time effects in the magnetic cooling method. *Proc. R. Soc. Lond. A* **155,** 629–639 (1936).
3. Van Vleck, J. H. Paramagnetic relaxation times for titanium and chrome alum. *Phys. Rev.* **57,** 426–447 (1940).
4. Gatteschi, D., Sessoli, R. & Villain, J. *Molecular Nanomagnets* (Oxford Univ. Press, 2006).
5. Villain, J., Hartman-Boutron, F., Sessoli, R. & Rettori, A. Magnetic relaxation in big magnetic molecules. *Europhys. Lett.* **27,** 159–164 (1994).
6. Garanin, D. A. & Chudnosvky, E. M. Thermally activated resonant magnetization tunneling in molecular magnets: Mn$_{12}$Ac and others. *Phys. Rev. B* **56,** 011102 (1997).
7. Leuenberger, M. & Loss, D. Spin relaxation in Mn$_{12}$-acetate. *Europhys. Lett.* **46,** 692–699 (1999).
8. Sessoli, R., Gatteschi, D., Caneschi, A. & Novak, N. A. Magnetic bistability of a metal-ion cluster. *Nature* **365,** 141–144 (1993).
9. Palyi, A., Struck, P. R., Rudner, M., Flensberg, K. & Burkard, G. Spin–orbit-induced strong coupling of a single spin to a nanomechanical resonator. *Phys. Rev. Lett.* **108,** 206811 (2012).
10. Kovalev, A., Hayden, L., Bauer, G. & Tscherkovniak, Y. Macrospin tunneling and magneto-polaritons with nanomechanical interference. *Phys. Rev. Lett.* **106,** 147203 (2011).
11. Garanin, D. A. & Chudnovsky, E. Quantum entanglement of a tunneling spin with mechanical modes of a torsional resonator. *Phys. Rev. X* **1,** 011005 (2011).
12. Laird, E., Pei, F., Tang, W., Steele, G. A. & Kouwenhoven L. P. A high quality factor carbon nanotube mechanical resonator at 39 GHz. *Nano Lett.* **12,** 193–197 (2011).
13. Peng, H. B., Chang, C. W., Aloni, S., Yuzvinsky, T. D. & Zettl, A. Ultrahigh frequency nanotube resonator. *Phys. Rev. Lett.* **97,** 087203 (2006).
14. Sapmaz, S., Jarillo-Herrero, P., Blanter, Y. M., Dekker, C. & van der Zant, H. S. J. Tunneling in suspended carbon nanotubes assisted by longitudinal phonons. *Phys. Rev. Lett.* **96,** 026801 (2006).
15. Huettel, A., Witkamp, B., Leijnse, M., Wegewijs, M. R. & van der Zant, H. S. J. Pumping of vibrational excitations in the Coulomb-blockade regime in a suspended carbon nanotube. *Phys. Rev. Lett.* **102,** 225501 (2009).
16. Leturcq, R. *et al.* Franck–Condon blockade in suspended carbon nanotube quantum dots. *Nature Phys.* **5,** 327–331 (2009).
17. Poot, M. & van der Zant, H. S. J. Mechanical systems in the quantum regime. *Phys. Rep.* **511,** 273–335 (2011).
18. Ganzhorn, M. & Wernsdorfer, W. Dynamics and dissipation induced by single electron tunneling in carbon nanotube nanoelectromechanical system. *Phys. Rev. Lett.* **108,** 175502 (2012).
19. Lassagne, B., Tarakanov, Y., Kinaret, J., Garcia-Sanchez, D. & Bachthold, A. Coupling mechanics to charge transport in carbon nanotube mechanical resonators. *Science* **325,** 1107–1110 (2009).
20. Steele, G. *et al.* Strong coupling between single electron tunneling and nanomechanical motion. *Science* **325,** 1103–1107 (2009).
21. Hüttel, A. K. Carbon nanotubes as ultrahigh quality factor mechanical resonators. *Nano Lett.* **9,** 2547–2552 (2009).
22. Lassagne, A., Garcia-Sanchez, D., Aguasca, A. & Bachtold, A. Ultrasensitive mass sensing with a nanotube electromechanical resonator. *Nano Lett.* **8,** 3735–3738 (2008).
23. Chiu, H., Hung, P., Postma, H. W. Ch. & Bockrath, M. Atomic scale mass sensing using carbon nanotube resonators. *Nano Lett.* **8,** 4342–4346 (2008).
24. Jensen, K., Kim, K. & Zettl, A. An atomic-resolution nanomechanical mass sensor. *Nature Nanotech.* **3,** 533–556 (2008).
25. Lassagne, B., Ugnati, D. & Respaud, M. Ultrasensitive magnetometers based on carbon nanotube mechanical resonators. *Phys. Rev. Lett.* **107,** 130801 (2011).
26. Bogani, L. & Wernsdorfer, W. Molecular spintronics using single-molecule magnets. *Nature Mater.* **7,** 179–186 (2008).
27. Heersche, H. *et al.* Electron transport through single Mn$_{12}$ molecular magnets. *Phys. Rev. Lett.* **96,** 206801 (2006).
28. Zyazin, A. S. *et al.* Electric field controlled magnetic anisotropy in a single molecule. *Nano Lett.* **10,** 3307–3311 (2010).
29. Vincent, R., Klyatskaya, S., Ruben, M., Wernsdorfer, W. & Balestro, F. Electronic readout of a single nuclear spin in a single molecule transistor. *Nature* **488,** 357–360 (2012).
30. Urdampilleta, M., Cleuziou, J-P., Klyatskaya, S., Ruben, M. & Wernsdorfer, W. Supramolecular spin valves. *Nature Mater.* **10,** 502–506 (2011).
31. Friedman, J. R., Sarachik, M. P., Tejada, J. & Ziolo, R. Macroscopic measurement of resonant magnetization tunnelling in high-spin molecules. *Phys. Rev. Lett.* **76,** 3830–3833 (1996).
32. Thomas, L. *et al.* Macroscopic quantum tunnelling of magnetization in a single crystal of nanomagnets. *Nature* **383,** 145–147 (1996).
33. Wernsdorfer, W. & Sessoli, R. Quantum phase interference and parity effects in magnetic molecular clusters. *Science* **284,** 133–135 (1999).
34. Takahashi, S. *et al.* Coherent manipulation and decoherence of S=10 single-molecule magnet. *Phys. Rev. Lett.* **102,** 087603 (2009).
35. Ishikawa, N., Sugita, M. & Wernsdorfer, W. Quantum tunneling of magnetization in lanthanide single-molecule magnets: bis(phthalocyaninato)terbium and bis(phthalocyaninato)dysprosium anions. *Angew. Chem. Int. Ed.* **44,** 2931–2935 (2005).
36. Kyatskaya, S. *et al.* Anchoring of rare-earth-based single-molecule magnets on single-walled carbon nanotubes. *J. Am. Chem. Soc.* **131,** 15143–15151 (2009).
37. Lopes, M. *et al.* Surface-enhanced Raman signal for terbium single-molecule magnets grafted on graphene. *ACS Nano* **4,** 7531–7536 (2010).
38. Chudnovsky, E., Garanin, D. A. & Schilling, R. Universal mechanism of spin relaxation in solids. *Phys. Rev. B* **72,** 094426 (2005).
39. Ohm, C., Stampfer, C., Splettstoesser, J. & Wegewijs, M. R. Readout of carbon nanotube vibrations based on spin–phonon coupling. *Appl. Phys. Lett.* **100,** 143103 (2012).

Acknowledgements

Author contributions

M.G. and W.W. designed, conducted and analysed the experiments. S.K. and M.R. designed, synthesized and characterized the molecule. M.G. and W.W. co-wrote the paper.

Additional information

Competing financial interests

The authors declare no competing financial interests.